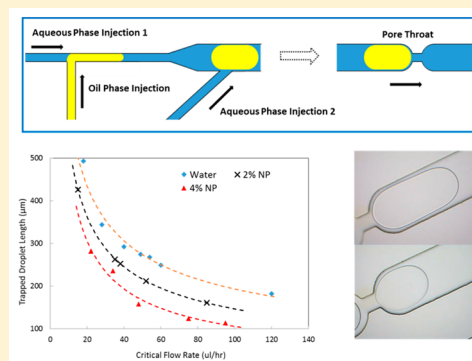


# Microfluidic Investigation of Nanoparticles' Role in Mobilizing Trapped Oil Droplets in Porous Media

Ke Xu, Peixi Zhu,\* Chun Huh, and Matthew T. Balhoff

Department of Petroleum and Geosystems Engineering, The University of Texas at Austin, Austin, Texas 78712, United States

**ABSTRACT:** The flow of multiple fluid phases in porous media often results in trapped droplets of the nonwetting phase. Recent experimental and theoretical studies have suggested that nanoparticle aqueous dispersions may be effective at mobilizing trapped droplets of nonwetting fluid (oil) in porous media. Hypotheses to explain the observation include the nanoparticles' modification of solid wettability, droplet stabilization, and changes in interfacial tension and interface rheology. However, because it is difficult to observe droplet behavior on the pore scale, how those factors contribute to oil droplet mobilization has not been fully understood. In this work, we investigated the nanoparticles' role in nanoparticle-based improved recovery of the nonwetting phase through the direct observation of the mobilization of trapped oil droplets in microfluidic structures that mimic pore–throat geometries. A microfluidic platform was constructed for this study, on which different displacing liquids including aqueous surfactant solutions and nanoparticle suspensions were tested. We found that the nanoparticle concentration is positively related to the oil mobilization efficiency. An approximate mathematical model for calculating the maximum size of an oil droplet trapped in a pore–throat geometry for a fixed flow rate matches the experiment result for displacing liquid with no nanoparticles. The model still holds when the nanoparticle suspension is a displacing liquid. We concluded that nanoparticles mobilize oil in these geometries in a mechanism similar to that for surfactants, which is an increase in capillary number rather than an effect of other fluidic or interfacial properties such as the dynamics adsorption of nanoparticle or dilational rheology of a nanoparticle-adsorbed interface.



## I. INTRODUCTION

Nanoparticles (NPs) possess many promising properties that render them with the potential for an easier mobilization of the nonwetting fluid in multi-phase flow, including applications such as enhanced oil recovery (EOR).<sup>1,2</sup> In an aqueous dispersion, NPs can be adsorbed on the fluid/fluid or fluid/solid interface because of the reduction of interfacial energy.<sup>3–7</sup> The adsorption leads to several effects that may help to reduce residual oil or increase the sweep efficiency: generation/stabilization of an emulsion/foam,<sup>8,9</sup> reduction of interfacial tension (IFT),<sup>5,10,11</sup> change in emulsion rheology,<sup>12–14</sup> increase in disjoining pressure,<sup>15,16</sup> and alteration of wettability.<sup>1,17,18</sup> As NPs are thermally and chemically more stable than polymer or surfactant,<sup>9,19,20</sup> and they can be effectively employed under harsh subsurface conditions.

A number of displacement experiments with reservoir cores or sand packs have been reported to investigate the role of NPs in mobilizing trapped oil. Hendraningrat et al.<sup>21</sup> injected a dispersion of silica NPs into sandstone cores after flooding them with brine. They showed improved oil recovery with the increase in NP concentration in the displacing phase, which was attributed to interfacial tension reduction and wettability alteration. The injection can lead to the adsorption of NPs on the rock surface, which is considered to be a key factor that alters wettability or reduces permeability.<sup>21–23</sup> NPs' effect on fluid rheology has also been investigated. Low concentrations (<5 wt %) of NPs do not significantly impact the aqueous

viscosity,<sup>24</sup> but core flood experiments show that NPs can be used as foam/emulsion stabilizing agents, thereby substantially increasing the apparent viscosity of the displacing phase.<sup>25,26</sup> Although the NP role in reducing residual oil has been claimed, the fundamental mechanisms for the mobilization of trapped oil using NP-based fluids is still not fully understood, partially because of the difficulty of directly visualizing of the mobilization process.<sup>1</sup>

Microfluidics provide a direct visualization of immiscible displacement behavior down to the micrometer scale. The development of fluid control theory/techniques in micrometer channels<sup>27</sup> and the reproducible processes for manufacturing microfluidic chips with complicated channel geometries<sup>28</sup> have led to the utilization of the technology in many miniaturized flow applications, such as chemical processes,<sup>29</sup> material synthesis,<sup>30</sup> and biological and chemical analysis.<sup>31,32</sup> In porous media, two-phase flow phenomena occur within pores and throats on the micrometer length scale. Therefore, microfluidics is an excellent tool for studying fundamental flow phenomena on the pore scale that could not be observed inside a rock sample. Recently, microfluidics have been used to study some fundamental flow phenomena in porous media including single-phase flow,<sup>33</sup> multiphase flow,<sup>34</sup> interfacial phenomena,<sup>35,36</sup> and

Received: October 7, 2015

Revised: December 1, 2015

Published: December 15, 2015

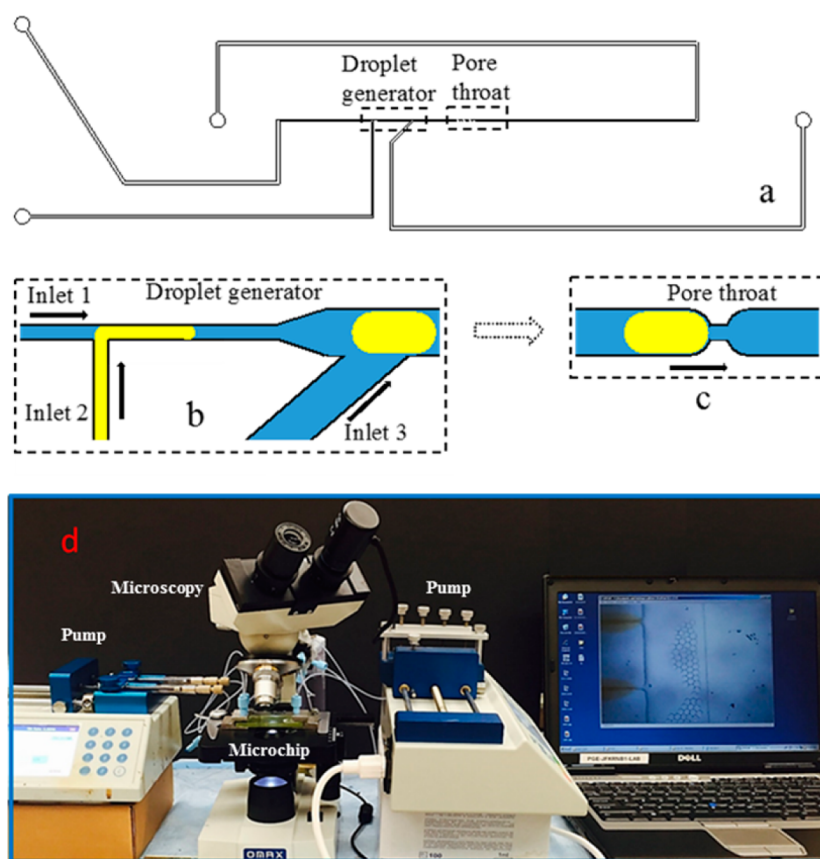


**Figure 1.** (a)–(c) Schematic diagram of the microfluidic design in this experiment. (a) Full view, (b) droplet generator, and (c) pore–throat structure. The aqueous phase is represented in blue, and the oil phase is represented in yellow. The arrows indicate the flow direction. The dimensions of the design are given in Table 1. (d) Image of the overall experimental setup.

emulsion behavior.<sup>37,38</sup> The displacement processes of oil recovery, such as water flooding,<sup>39</sup> foam flooding,<sup>40</sup> and polymer/surfactant flooding,<sup>39,3</sup> have also been investigated by using a 2D microfluidics porous network (also called a micromodel), that is analogous to core flood tests but with the advantage of fluid flow visualization.

A few works on NP-based EOR have also been presented in a 2D microfluidics porous network.<sup>41–44</sup> Li et al.<sup>45</sup> injected an NP dispersion in secondary oil recovery. They showed that steady-state interfacial tension between a nanofluid and oil decreases with an increase in NP concentration and that increased NP concentration is positively related to final oil recovery. The deposition of NPs on the solid surface and its positive effect on surface wettability were also visualized.<sup>41,43</sup> Nguyen et al. showed the improvement of oil recovery over water flooding when NP-stabilized CO<sub>2</sub> foam was used as the displacing phase.<sup>20</sup> These works have given a better understanding of flow behavior in the pore structure. However, their focuses are mostly on the overall effect of NPs on oil recovery rather than on understanding the oil trapping and mobilization mechanism in the single pore-structure unit. Scenarios of trapped oil on the pore scale include the trapping of oil droplets in pore–throat geometries, attachment to the solid surface, oil unmobilized in micrometer-scale low-permeability zones, and so forth. Mechanisms of oil mobilization in different scenarios may be different, and distinguishing them is difficult when the interconnected flow paths are considered to be a continuum medium.

Immobilized oil in pore–throat geometries in the form of droplets arises from the presence of capillary forces and is one of the most common oil-trapping scenarios in water-wet porous media.<sup>46</sup> It is therefore important to understand whether and how NPs affect the trapping and mobilization of oil droplets. For pure water and surfactant solutions as a continuous phase, it has been well established that interfacial tension (IFT) and viscosity are two key factors in determining droplet trapping and mobilization.<sup>47,48</sup> For NP dispersions, although a positive relationship between the reduction of IFT and the final oil recovery has been shown,<sup>45</sup> it is unproven that IFT rather than other potential mechanisms such as wettability modification<sup>18</sup> and interface dilational rheology change<sup>14</sup> is the dominant mechanism. Furthermore, an NP aqueous suspension is considerably different from water or a surfactant aqueous solution in at least two aspects in an oil-in-water system: (1) IFT of the nanofluid–oil interface may not be constant during droplet generation or deformation, which are common occurrences in porous media. This dynamic IFT phenomenon is due to the NP's much lower diffusivity compared to that of surfactant molecules, which makes the adsorption of NPs on a fluid–fluid interface much slower than for surfactant. For instance, in pendant drop experiments, the typical time scale for reaching equilibrium IFT between oil and an NP dispersion is on the order of 10<sup>3</sup> s, whereas the time scale for a surfactant system is several orders of magnitude lower.<sup>11,49</sup> (2) NPs adsorbed on a liquid–liquid interface may form a network, manifested as a change in interface dilational rheology,<sup>14</sup> that

may affect the deformation of droplets and then affect the droplet-trapping mechanisms.

In this work, we attempted to better understand the role of NPs in mobilizing trapped nonwetting phase (oil) droplets in a pore–throat structure by constructing a microfluidic chip with well-defined pore–throat geometry. We also developed a mathematical model to describe droplet trapping criteria with parameters that are easily obtainable, and the model was validated by experimental data. By comparing the model against experimental results of a system with NP in the continuous phase, we clarified that the model was also valid when adding NP to the displacing fluid, and thus we provide an explanation of how NPs help to mobilize trapped oil droplets on the pore scale. Applications of this work include food processing and the chemical industry and environmental engineering, where phenomena such as oil–water separation with a microporous membrane,<sup>50</sup> emulsification with a porous membrane,<sup>51</sup> and multiphase flow in packed-bed reactors<sup>52</sup> may occur and multiphase flow through throatlike geometries may be manifest.

## II. MATERIALS AND METHODS

**II.1. Materials and Microfluidic Platform.** In our microfluidic experiments, decane or a surfactant (Span 80, TCI AMERICA) in decane solution was used as the oil phase, and DI water or an NP dispersion was used as the aqueous phase to displace the trapped oil. The surfactant-in-decane solution was prepared by adding a specific amount of surfactant in decane. The silica NP (EORSX, provided by Nissan Chemical) used in this work has an average size of 5 nm. The NPs are provided as a 20 wt % concentrated dispersion and were diluted to achieve the desired concentrations (2 and 4 wt % in this work).

The 2D design of the microfluidic chip is given in Figure 1a. The two major features in this design are the droplet generator (Figure 1b) and the pore–throat structure (Figure 1c). The droplet generator consists of three independent flow inlets. Upstream is a typical T junction for creating monodisperse oil-in-water emulsion droplets.<sup>34,53</sup> The size and generation frequency of the droplets can be controlled by adjusting the injection rates of the aqueous (inlet1) and oil phases (inlet2).<sup>34</sup> The main channel is then widened downstream from the T junction. We set another aqueous-phase injection inlet (inlet3), with the help of which we could have good control of the total flow rate and volume ratio. Further downstream is the pore–throat structure for oil droplet trapping. The channel width converges dramatically from 230 to 50  $\mu\text{m}$  and then expands back to 230  $\mu\text{m}$ , as shown in Figure 1c.

Glass was used as the microfluidic material. The chip fabrication followed a standard lithography process and hydrofluoric (HF) acid etching process. A channel depth of 30  $\mu\text{m}$  was obtained by controlling the HF-etching time. The dimensions of the channels after etching are given in Table 1. The etched glass piece was bonded

**Table 1. Channel Dimensions in the Microfluidic Device**

channel	width ( $\mu\text{m}$ )	depth ( $\mu\text{m}$ )
inlet 1	40	30
inlet 2	40	30
inlet 3	230	30
main channel	230	30
throat	50	30

to a cover piece by heating to 690 °C. A sample of the bonded chip is shown in Figure 1d. Because of the isotropic etching of HF, the cross-section of the channel is not strictly rectangular but somewhat trapezoidal.

**II.2. Flow Experiment.** The microfluidic device was placed on an optical microscope (OMAX) platform. The three flow inlets were connected to three independent syringes (Hamilton), which were

mounted on three syringe pumps (Chemyx Fusion) that allow precise control of the injection flow rate. The experimental setup is shown in Figure 1d.

In our microfluidic experiment, emulsion droplets with an expected initial size were first generated by adjusting the flow rate of flow inlets 1 and 2 (Figure 2a). After the flow became stable, the oil injection of inlet 2 was paused and the flow rate of aqueous phase injection inlet 3 was increased in order to push all droplets through the throat except the last one. Before the last droplet arrived at the throat, flow from inlet 3 was paused and the flow rate of the aqueous phase from inlet 1 was reduced to 5  $\mu\text{L}/\text{h}$ . In the operating range of this experiment, all droplets could be trapped at the throat at this flow rate (Figure 2b,c). Then, the flow rate of inlet 1 was increased gradually until the droplet was pushed through the throat. The flow rate was recorded as the critical flow rate for that trapped droplet size. Then, we repeated the above procedures for a different initial oil droplet size and finally obtained a critical flow rate versus droplet size relationship for different systems. Figure 2 shows snapshots taken during the experiments. Monodisperse droplets generated from the T junction are shown in Figure 2a. Oil droplets of different sizes trapped at the throat are shown in Figure 2b,c. In all experiments, droplets take a slug shape, i.e., have an equivalent diameter larger than the channel width. The total experimental duration from droplet generation to the point when the droplet passes through the constriction is on the order of tens of seconds.

## III. RESULTS AND DISCUSSION

**III.1. Effects of NPs in Reducing Trapped Oil Droplet Size.** Figure 3 shows the length of the trapped droplet  $L$  along the principal flow direction against a critical flow rate,  $Q$ , for 0 wt % (DI water) and 2 and 4 wt % NP dispersions. The definition of  $L$  is provided in Figure 2b. The monotonically decreasing relation indicates that smaller droplets are more difficult to mobilize, i.e., when the droplet size gets smaller, a higher flow rate is required to mobilize it through the throat. This is due to the increase in capillary resistance force caused by increased droplet curvature. It is consistent with the fact that the increase in the capillary number recovers more oil.

A comparison of the three curves in Figure 3 shows better oil recovery with the increase in NP concentration. When the critical flow rate of the aqueous phase is fixed at 50  $\mu\text{L}/\text{h}$ , for example, the dashed curves indicate that the smallest size of the droplet that can be mobilized in 0, 2, and 4 wt % dispersion is 280, 210, and 160  $\mu\text{m}$ , respectively. Therefore, the size of unrecoverable oil droplet is decreased by 40% when the NP concentration is increased from 0 to 4 wt %. The results suggest that the presence of NPs in the aqueous phase has the potential to enhance oil recovery by pushing trapped oil droplets in the pore–throat structure that cannot be mobilized by water, consistent with the results of core flood experiments.<sup>1,21,22</sup>

In many previous works, researchers suggested that the reduction of interfacial tension due to the adsorption of NPs at the fluid interface may be a critical mechanism. However, other hypotheses (e.g., dynamic IFT in the presence of NP and changes in other interfacial properties such as dilational rheology of the NP-adsorbed interface<sup>14</sup>) need to be investigated.

In section III.2, we present a semiempirical correlation that well describes a droplet displacement process when the change in IFT is the only factor that governs the interfacial effect. The correlation was first validated in a dilute surfactant system and then applied to the case with the NP dispersion. If the data from the latter matches the model, we could then conclude that the reduction of the IFT is the major reason for droplet

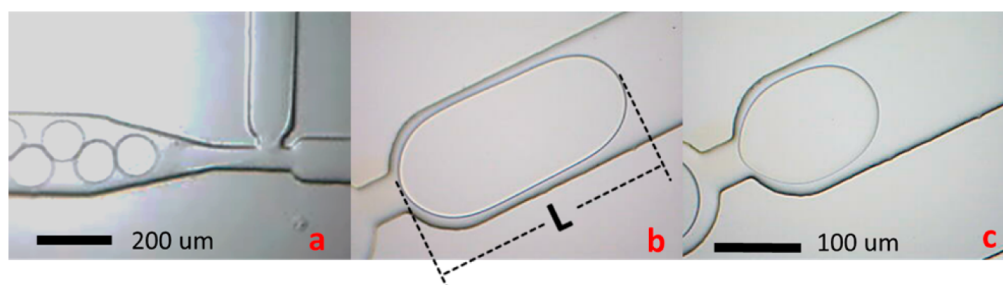


**Figure 2.** Snapshots showing droplet formation and trapping in the microfluidic chip. (a) Monodisperse droplets generated at the T junction. (b, c) Oil droplets of different sizes trapped at the throat and the definition of droplet length. (b) and (c) share the same scale bar as shown in (c). The flow direction is from right to left.

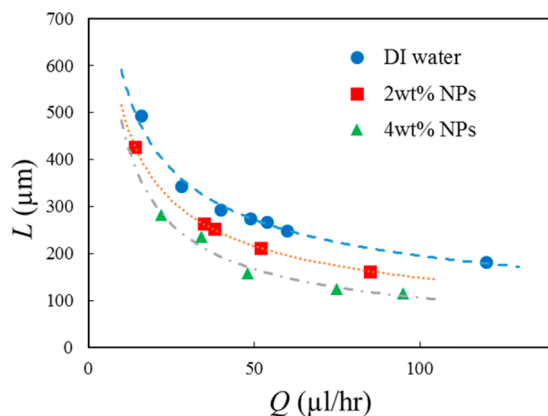


**Figure 3.** Plot of trapped droplet size  $L$  versus critical flow rate  $Q$ . Blue circles are data for DI water as the aqueous phase; red squares are data for 2 wt % NPs in water as the aqueous phase; and green triangles are data for 4 wt % NPs in water as the aqueous phase. The dotted lines are a simple power fitting of three groups of data. The curves are presented merely to show the trend in the data.

mobilization. Otherwise, it implies the existence of other interfacial mechanisms.

**III.2. Correlation Description.** A simplified force balance analysis on the dynamics of the droplet being trapped in a pore–throat geometry is not known to be available. There are relevant works on the dynamics of elongated droplet (slug) flows in straight microchannels, moving along with the surrounding medium, with IFT being the only interfacial effect considered.<sup>29,54</sup> According to those works, the physical forces exerted on an oil droplet include the hydrodynamic force,  $F_{\text{hydrod}}$ , that tends to mobilize the droplet, and a capillary force,  $F_{\text{caps}}$ , that is a result of droplet deformation induced by the hydrodynamic force.  $F_{\text{hydrod}}$  is proportional to the droplet length  $L$ , the velocity of the continuous fluid  $u$ , and the viscosity of continuous fluid  $\mu$  as

$$F_{\text{hydrod}} = a\mu uL \quad (1)$$

where  $a$  is the geometric coefficient of the rectangular channel.

$F_{\text{caps}}$  is a more complex force, which is related to both the interface properties and the continuous viscous force. As indicated in ref 54, it can be expressed by eq 2 as

$$F_{\text{caps}} = b\mu Ca^{-1/3} \quad (2)$$

where  $b$  is a geometric coefficient of the rectangular channel and  $Ca$  is the capillary number, defined here as

$$Ca = \frac{\mu u}{\gamma} \quad (3)$$

where  $\gamma$  is the water–oil interfacial tension.

We assume that eqs 1 and 2 are also applicable for a trapped oil droplet at the throat, with the channel's variable cross-section represented by geometric factors  $a$  and  $b$ . Because the droplet is at rest, the hydrodynamic force balances the capillary force. Therefore, we have  $F_{\text{hydrod}} = F_{\text{caps}}$ , which leads to

$$L \propto Ca^{-1/3} \quad (4)$$

Equation 4 should hold when the droplet trapped at the throat is static and experiences only hydrodynamic and capillary forces.

**III.3. Model Validation with Deionized Water and Surfactant Solutions.** For a fixed geometry, the slope of eq 4 should be constant regardless of the liquids used. To validate the model, we performed the experiment using deionized water as the continuous phase and decane mixed with different concentrations of surfactant (Span 80) as the dispersed phase in the same chip. Here we chose to use an oil-soluble surfactant in the droplet phase because if water-soluble surfactant were used in the continuous phase the wettability of the channel could be altered by the surfactant adsorption and the viscosity of the continuous phase could be changed. The concentrations of Span 80 and the corresponding equilibrium IFT (required for the calculation of  $Ca$ ) are provided in Table 2.

**Table 2.** Concentrations of Surfactant and NP in the Experiment and the Corresponding IFT Data

Span 80 (wt %)	IFT (mN/m)	NP (wt %)	IFT (mN/m)
0	48.3	0	48.3
0.0045	28	2	33.0
1	4.2	4	29.9

Figure 4 shows plots of droplet length  $L$  versus  $Ca^{-1/3}$  for various concentrations of surfactant in the oil phase. Regardless of the surfactant concentration in the oil phase, all of the data points fall on a straight line, indicating that the correlation of eq 4 is valid when viscosity and IFT are the only dominating factors for oil trapping.

**III.4. Model Fitting with an Aqueous NP Suspension.** We then used eq 4 to fit to the data obtained from the NP flow experiments. A good fit would indicate that the reduction of IFT is the main effect contributed by NPs to mobilize trapped oil. Otherwise, other interfacial effects may also make significant contributions. The fitting results are presented in Figure 5a. The linear Einstein equation for effective viscosity, which is

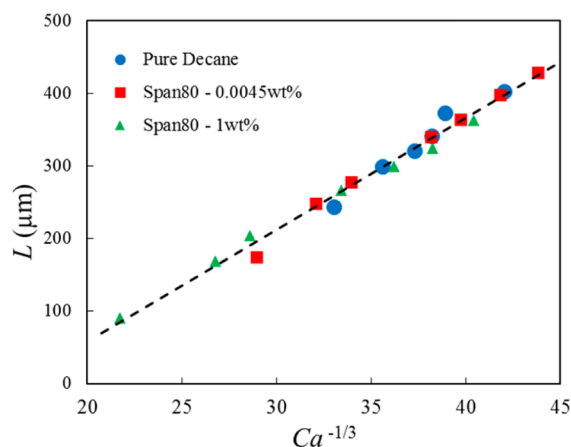


**Figure 4.** Fitting result of eq 4 to a surfactant system. DI water was used as the aqueous phase. Blue circles are data for pure decane as the oil phase; red squares are data for  $4.5 \times 10^{-3}$  wt % Span80 in decane as the oil phase; and green triangles are data for 1 wt % Span80 in decane as the oil phase. The linear fitting is given by the black dashed line.

applicable to an NP suspension for this concentration range, was used to calculate  $Ca$ . The IFT values between decane and different concentrations of NP dispersion are listed in Table 2 along with the data for the surfactant system. As was observed for surfactant, all of the data in Figure 5 collapse onto a straight line, suggesting that the effect of NPs on mobilizing the trapped oil droplet is mainly through the reduction of IFT, which increases the capillary number.

Figure 5b shows the dynamic interfacial tension between the NP dispersion and decane measured by the pendant drop method. It shows that the time scale to reach the equilibrium IFT is on the order of  $10^3$  s, which is consistent with the published works.<sup>55,56</sup> However, the time scale from droplet generation to trapping in the microfluidic channel is approximately on the order of 10 s. This indicates that the diffusion time is no longer significant and the adsorption of NPs on the interface is significantly expedited possibly by the presence of flow.

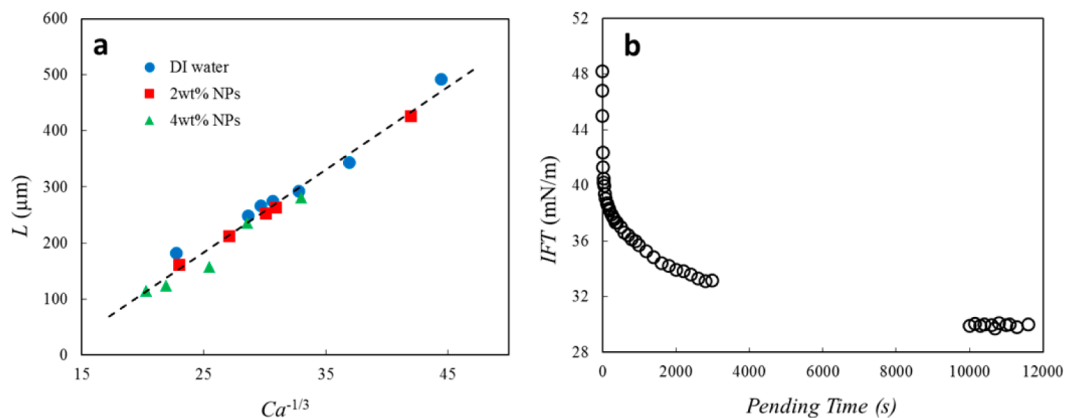


**Figure 5.** (a) Data fitting of the oil-trapping experiment with NP in the aqueous phase. Blue circles are data for DI water as the aqueous phase; orange triangles are data for 2 wt % NPs in water as the aqueous phase; and red squares are data for 4 wt % NPs in water as the aqueous phase. The black dashed line shows the linear correlation. (b) Plot of IFT versus time between the NP aqueous suspension and oil in a pending drop test with oil as the dispersed phase.

## IV. CONCLUSIONS

A microfluidics platform to investigate the mechanism of an oil droplet trapped at a pore–throat structure was constructed, with precise control of the flow conditions. We found that an increase in NP concentration could decrease the flow rate required to push a certain oil droplet out on a fixed geometry, which means an easier oil recovery process.

A mathematical model was constructed and successfully correlates the oil droplet size with the critical flow condition to mobilize the droplet under the condition that the capillary number and pore–throat geometry are the only two dominant parameters.

Nanoparticle's role in mobilizing trapped oil droplets at a pore–throat geometry was clarified on the basis of this model. We found that aqueous NP suspensions also fit the correlation, indicating that no factors other than capillary number and pore geometry play a considerable role in this case. In mobilizing an oil droplet trapped in the pore–throat structure, the NP's effect is very similar to that of surfactant; i.e., it reduced the trapped oil size mainly by reducing IFT. In addition, we also found that NP's adsorption to the oil–water interface is considerably accelerated in the presence of flow, so the dynamic IFT effect is not significant.

## AUTHOR INFORMATION

### Corresponding Author

\*E-mail: zpeixi@utexas.edu.

### Notes

The authors declare no competing financial interest.

## ACKNOWLEDGMENTS

We gratefully acknowledge support from the sponsors of the Nanoparticles for Subsurface Engineering Industrial Affiliates Project at the University of Texas at Austin.

## REFERENCES

- Bennetzen, M. V.; Mogensen, K. *Novel Applications of Nanoparticles for Future Enhanced Oil Recovery. International Petroleum Technology Conference*; Kuala Lumpur, Malaysia, 2014.
- Hashemi, R.; Nassar, N. N.; Pereira Almaso, P. Nanoparticle technology for heavy oil in-situ upgrading and recovery enhancement: Opportunities and challenges. *Appl. Energy* **2014**, *133*, 374–387.

- (3) Aktas, F.; Clemens, T.; Castanier, L.; Kovscek, A. R. Viscous Oil Displacement via Aqueous Associative Polymers. SPE Symposium on Improved Oil Recovery; Society of Petroleum Engineers: Tulsa, OK, 2008.
- (4) Bhattacharya, R.; Basu, J. K. Microscopic dynamics of nanoparticle monolayers at air-water interface. *J. Colloid Interface Sci.* **2013**, *396*, 69–74.
- (5) Du, K.; Glogowski, E.; Emrick, T.; Russell, T. P.; Dinsmore, A. D. Adsorption energy of nano- and microparticles at liquid-liquid interfaces. *Langmuir* **2010**, *26*, 12518–12522.
- (6) Okada, M.; Maeda, H.; Fujii, S.; Nakamura, Y.; Furuzono, T. Formation of Pickering emulsions stabilized via interaction between nanoparticles dispersed in aqueous phase and polymer end groups dissolved in oil phase. *Langmuir* **2012**, *28*, 9405–9412.
- (7) Zoueshtiagh, F.; Baudoin, M.; Guerrin, D. Capillary tube wetting induced by particles: towards armoured bubbles tailoring. *Soft Matter* **2014**, *10*, 9403–9412.
- (8) Hunter, T. N.; Pugh, R. J.; Franks, G. V.; Jameson, G. J. The role of particles in stabilising foams and emulsions. *Adv. Colloid Interface Sci.* **2008**, *137*, 57–81.
- (9) Nallamilli, T.; Mani, E.; Basavaraj, M. G. A model for the prediction of droplet size in Pickering emulsions stabilized by oppositely charged particles. *Langmuir* **2014**, *30*, 9336–9345.
- (10) Bizmark, N.; Ioannidis, M. A.; Henneke, D. E. Irreversible adsorption-driven assembly of nanoparticles at fluid interfaces revealed by a dynamic surface tension probe. *Langmuir* **2014**, *30*, 710–717.
- (11) Rana, S.; Yu, X.; Patra, D.; Moyano, D. F.; Miranda, O. R.; Hussain, I.; Rotello, V. M. Control of surface tension at liquid-liquid interfaces using nanoparticles and nanoparticle-protein complexes. *Langmuir* **2012**, *28*, 2023–2027.
- (12) Sagis, L. M. C. Dynamic properties of interfaces in soft matter: Experiments and theory. *Rev. Mod. Phys.* **2011**, *83*, 1367–1403.
- (13) Schmitt, M.; Limage, S.; Grigoriev, D. O.; Kragel, J.; Dutschk, V.; Vincent-Bonnieu, S.; Miller, R.; Antoni, M. Transition from spherical to irregular dispersed phase in water/oil emulsions. *Langmuir* **2014**, *30*, 4599–4604.
- (14) Ravera, F.; Ferrari, M.; Liggieri, L.; Loglio, G.; Santini, E.; Zanobini, A. Liquid-liquid interfacial properties of mixed nanoparticle-surfactant systems. *Colloids Surf., A* **2008**, *323*, 99–108.
- (15) Wasan, D. T.; Nikolov, A. D. Spreading of nanofluids on solids. *Nature* **2003**, *423*, 156–159.
- (16) Nikolov, A.; Kondiparty, K.; Wasan, D. Nanoparticle self-structuring in a nanofluid film spreading on a solid surface. *Langmuir* **2010**, *26*, 7665–7670.
- (17) Sajeesh, P.; Sen, A. K. Particle separation and sorting in microfluidic devices: a review. *Microfluid. Nanofluid.* **2014**, *17*, 1–52.
- (18) Giraldo, J.; Benjumea, P.; Lopera, S.; Cortés, F. B.; Ruiz, M. A. Wettability Alteration of Sandstone Cores by Alumina-Based Nanofluids. *Energy Fuels* **2013**, *27*, 3659–3665.
- (19) Maini, B. B.; Ma, V. Thermal Stability of Surfactants for Steamflood Applications. SPE Oilfield and Geothermal Chemistry Symposium; Society of Petroleum Engineers: Phoenix, AZ, 1985.
- (20) Yu, W.; Xie, H. A Review on Nanofluids: Preparation, Stability Mechanisms, and Applications. *J. Nanomater.* **2012**, *2012*, 1–17.
- (21) Hendraningrat, L.; Li, S.; Torsæter, O. A coreflood investigation of nanofluid enhanced oil recovery. *J. Pet. Sci. Eng.* **2013**, *111*, 128–138.
- (22) Ogolo, N. A.; Olafuyi, O. A.; Onyekonwu, M. O. Enhanced Oil Recovery Using Nanoparticles. SPE Saudi Arabia Section Technical Symposium and Exhibition; Society of Petroleum Engineers: Al-Khobar, Saudi Arabia, 2012.
- (23) Zhang, T.; Murphy, M. J.; Yu, H.; Bagaria, H. G.; Yoon, K. Y.; Nielson, B. M.; Bielawski, C. W.; Johnston, K. P.; Huh, C.; Bryant, S. L. Investigation of nanoparticle adsorption during transport in porous media. *SPE J.* **2015**, *20*, 667–677.
- (24) Metin, C.; Bonnacaze, R.; Nguyen, Q. The Viscosity of Silica Nanoparticle Dispersions in Permeable Media. *SPE Reservoir Eval. Eng.* **2013**, *16*, 327–332.
- (25) Yu, J.; An, C.; Mo, D.; Liu, N.; Lee, R. L. Foam Mobility Control for Nanoparticle-Stabilized Supercritical CO<sub>2</sub> Foam. SPE Improved Oil Recovery Symposium; Society of Petroleum Engineers: Tulsa, OK, 2012.
- (26) Espinoza, D. A.; Caldelas, F. M.; Johnston, K. P.; Bryant, S. L.; Huh, C. Nanoparticle-Stabilized Supercritical CO<sub>2</sub> Foams for Potential Mobility Control Applications. SPE Improved Oil Recovery Symposium; Society of Petroleum Engineers: Tulsa, OK, 2010.
- (27) Abgrall, P.; Gué, A. M. Lab-on-chip technologies: making a microfluidic network and coupling it into a complete microsystem—a review. *J. Micromech. Microeng.* **2007**, *17*, R15–R49.
- (28) Stone, H. A.; Stroock, A. D.; Ajdari, A. Engineering Flows in Small Devices. *Annu. Rev. Fluid Mech.* **2004**, *36*, 381–411.
- (29) Song, H.; Ismagilov, R. F. Millisecond Kinetics on a Microfluidic Chip Using Nanoliters of Reagents. *J. Am. Chem. Soc.* **2003**, *125*, 14613–14619.
- (30) Xu, J.-H.; Zhao, H.; Lan, W.-J.; Luo, G.-S. A Novel Microfluidic Approach for Monodispersed Chitosan Microspheres with Controllable Structures. *Adv. Healthcare Mater.* **2012**, *1*, 106–111.
- (31) Nilghaz, A.; Wicaksono, D. H. B.; Gustiono, D.; Abdul Majid, F. A.; Supriyanto, E.; Abdul Kadir, M. R. Flexible microfluidic cloth-based analytical devices using a low-cost wax patterning technique. *Lab Chip* **2012**, *12*, 209–218.
- (32) Martinez, A. W.; Phillips, S. T.; Whitesides, G. M.; Carrilho, E. Diagnostics for the Developing World: Microfluidic Paper-Based Analytical Devices. *Anal. Chem.* **2010**, *82*, 3–10.
- (33) Koo, J.; Kleinstreuer, C. Liquid flow in microchannels: experimental observations and computational analyses of microfluidics effects. *J. Micromech. Microeng.* **2003**, *13*, 568–579.
- (34) Xu, J. H.; Li, S. W.; Tan, J.; Wang, Y. J.; Luo, G. S. Preparation of highly monodisperse droplet in a T-junction microfluidic device. *AIChE J.* **2006**, *52*, 3005–3010.
- (35) Xu, J. H.; Dong, P. F.; Zhao, H.; Tostado, C. P.; Luo, G. S. The dynamic effects of surfactants on droplet formation in coaxial microfluidic devices. *Langmuir* **2012**, *28*, 9250–9258.
- (36) Lee, H.; Lee, S. G.; Doyle, P. S. Photopatterned oil-reservoir micromodels with tailored wetting properties. *Lab Chip* **2015**, *15*, 3047–3055.
- (37) Xu, K.; Ge, X.-H.; Huang, J.-P.; Dang, Z.-X.; Xu, J.-H.; Luo, G.-S. A region-selective modified capillary microfluidic device for fabricating water-oil Janus droplets and hydrophilic-hydrophobic anisotropic microparticles. *RSC Adv.* **2015**, *5*, 46981–46988.
- (38) Shah, R. K.; Shum, H. C.; Rowat, A. C.; Lee, D.; Agresti, J. J.; Utada, A. S.; Chu, L.-Y.; Kim, J.-W.; Fernandez-Nieves, A.; Martinez, C. J.; Weitz, D. A. Designer emulsions using microfluidics. *Mater. Today* **2008**, *11*, 18–27.
- (39) Chang, L.-C.; Tsai, J.-P.; Shan, H.-Y.; Chen, H.-H. Experimental study on imbibition displacement mechanisms of two-phase fluid using micro model. *Environ. Earth Sci.* **2009**, *59*, 901–911.
- (40) Ma, K.; Lontas, R.; Conn, C. A.; Hirasaki, G. J.; Biswal, S. L. Visualization of improved sweep with foam in heterogeneous porous media using microfluidics. *Soft Matter* **2012**, *8*, 10669–10675.
- (41) Hendraningrat, L.; Li, S.; Suwarno; Torsæter, O. A Glass Micromodel Experimental Study of Hydrophilic Nanoparticles Retention for EOR Project. SPE Russian Oil and Gas Exploration and Production Technical Conference and Exhibition; Society of Petroleum Engineers: Moscow, Russia, 2012.
- (42) Lele, P.; Fadaei, H.; Guerrero, U.; Sinton, D. Development of a Microfluidic Device for Rapid Assessment of EOR Additives. SPE Heavy Oil Conference-Canada; Society of Petroleum Engineers: Calgary, Alberta, Canada, 2014.
- (43) Li, S.; Torsæter, O. An Experimental Investigation of EOR Mechanisms for Nanoparticles Fluid in Glass Micromodel. International Symposium of the Society of Core Analysts: Avignon, France, 2014.
- (44) Nguyen, P.; Fadaei, H.; Sinton, D. Nanoparticle Stabilized CO<sub>2</sub> in Water Foam for Mobility Control in Enhanced Oil Recovery via Microfluidic Method. SPE Heavy Oil Conference-Canada; Society of Petroleum Engineers: Calgary, Alberta, Canada, 2014.

- (45) Ryles, R. G. Chemical stability limits of water-soluble polymers used in oil recovery processes. *SPE Reservoir Eng.* **1988**, *3*, 23–34.
- (46) Yadali Jamaloei, B.; Kharrat, R. Analysis of Microscopic Displacement Mechanisms of Dilute Surfactant Flooding in Oil-wet and Water-wet Porous Media. *Transp. Porous Media* **2010**, *81*, 1–19.
- (47) Li, Y.; Wardlaw, N. C. Mechanisms of Nonwetting Phase Trapping during Imbibition at Slow Rates. *J. Colloid Interface Sci.* **1986**, *109*, 473–486.
- (48) Wang, X.; Wang, K.; Riaud, A.; Wang, X.; Luo, G. Experimental study of liquid/liquid second-dispersion process in constrictive microchannels. *Chem. Eng. J.* **2014**, *254*, 443–451.
- (49) Xu, K.; Xu, J.-H.; Lu, Y.-C.; Luo, G.-S. Extraction-Derived Self-Organization of Colloidal Photonic Crystal Particles within Confining Aqueous Droplets. *Cryst. Growth Des.* **2013**, *13*, 926–935.
- (50) Karnik, S. V.; Hatalis, M. K.; Kothare, M. V. Towards a palladium micro-membrane for the water gas shift reaction: Micro-fabrication approach and hydrogen purification results. *J. Microelectromech. Syst.* **2003**, *12*, 93–100.
- (51) Joscelyne, S. M.; Trägårdh, G. Membrane emulsification—a literature review. *J. Membr. Sci.* **2000**, *169*, 107–117.
- (52) Losey, M. W.; Schmidt, M. A.; Jensen, K. F. Microfabricated multiphase packed-bed reactors: characterization of mass transfer and reactions. *Ind. Eng. Chem. Res.* **2001**, *40*, 2555–2562.
- (53) Fu, T.; Ma, Y.; Funfschilling, D.; Li, H. Z. Dynamics of bubble breakup in a microfluidic T-junction divergence. *Chem. Eng. Sci.* **2011**, *66*, 4184–4195.
- (54) Fuerstman, M. J.; Lai, A.; Thurlow, M. E.; Shevkoplyas, S. S.; Stone, H. A.; Whitesides, G. M. The pressure drop along rectangular microchannels containing bubbles. *Lab Chip* **2007**, *7*, 1479–1489.
- (55) Santini, E.; Guzmán, E.; Ferrari, M.; Liggieri, L. Emulsions stabilized by the interaction of silica nanoparticles and palmitic acid at the water–hexane interface. *Colloids Surf, A* **2014**, *460*, 333–341.
- (56) Song, Y.; Luo, M.; Dai, L. L. Understanding nanoparticle diffusion and exploring interfacial nanorheology using molecular dynamics simulations. *Langmuir* **2010**, *26*, 5–9.